Composites: Part A 163 (2022) 107206

Contents lists available at ScienceDirect

Composites Part A

journal homepage: www.elsevier.com/locate/compositesa

Investigating the fatigue behaviour of quasi-isotropic pseudo-ductile thin-ply carbon/glass epoxy hybrid composites

Mohamad Fotouhi [a,*], Putu Suwarta [c,d], Ali Tabatabaeian [b], Sakineh Fotouhi [b], Ross Jenkin [c], Meisam Jalalvand [e], Michael R. Wisnom [c]

[a] Department of Materials, Mechanics, Management and Design, Delft University of Technology, Delft, the Netherlands
[b] James Watt School of Engineering, University of Glasgow, Glasgow G12 8QQ, UK
[c] Bristol Composites Institute, University of Bristol, Queen's Building, University Walk, Bristol BS8 1TR, UK
[d] Department of Mechanical Engineering, Institut Teknologi Sepuluh Nopember, Surabaya 60111, Indonesia
[e] Engineering Materials, School of Engineering, University of Southampton, SO17 1BJ Southampton, United Kingdom

ARTICLE INFO

Keywords:
Hybrid composites
Fatigue analysis
Un-notched
Open-hole
Pseudo-ductility

ABSTRACT

This paper investigates the fatigue behaviour of pseudo-ductile Quasi-Isotropic (QI) interlayer hybrids with un-notched and open-hole configurations. Two different types of QI pseudo-ductile hybrids were evaluated; HighC, with carbon to glass thickness ratio of 0.29, that is made of thin-ply M46JB-carbon/epoxy and thin-ply Xstrand-glass/epoxy prepregs, and LowC, with carbon to glass thickness ratio of 0.19, that is made of thin-ply T300-carbon/epoxy and standard-ply S-glass/epoxy prepregs. The hybrid configurations were loaded at 4 Hz in tension–tension fatigue without any initial damage and at different percentages of the pseudo-yield stress (σ_{py}) at which damage initiates. It was observed that there is no stiffness reduction, after 100,000 cycles, for a stress level of 80 % and 50 % of the σ_{py} for the un-notched and open-hole laminates, respectively. By increasing the stress level to 90 % and 70 % of the σ_{py} for the un-notched and open-hole laminates, respectively, there is a gradual stiffness reduction due to the appearance of matrix cracking and delamination in LowC, but no gradual reduction and no visible damage were observed for HighC. The final failure is more brittle and happens at a lower number of cycles for HighC compared with LowC. Different damage extents were observed for the investigated laminates before the final sudden failure due to variables such as the ply thickness, the cyclic energy release rate and the interfacial fracture toughness.

1. Introduction

Pseudo-ductile hybrid (PDH) composites have recently been introduced as a new generation of FRP composites to address the sudden and unexpected failure [1–3]. Different techniques and material combinations have been used to generate PDH composites. This includes hybridising conventional composites such as glass or carbon fibres reinforced thermoset/thermoplastics with metal fibres such as steel [4,5], or hybridizing thin-ply low-strain FRPs with thin-ply or conventional high-strain FRPs [3,6]. The available research on PDH composites suggests a relatively safe and gradual metal-like failure [7,8], with a visually detectable warning before the final failure [8].

PDH composites can outperform conventional carbon or glass fibre composites if designed properly [6,9]. Unidirectional (UD) and Quasi Isotropic (QI) thin-ply hybrids with different types of low strain and high strain fibres were introduced that generated the desired nonlinear stress–strain response and pseudo-ductility to avoid catastrophic failure [3,10]. Appropriate material properties, and suitable values of relative thickness, i.e., the thickness ratio of low strain material to high strain material and absolute thickness of low strain material, should be selected for an optimal PDH design [6]. A new lay-up concept to address the free-edge delamination in multi-directional/QI PDH composites, orientation-dispersed lay-up, was introduced in [11,12], where the finite element predictions were supported by experimental results, proving the reliability of the proposed lay-up arrangement under tension in all fibre orientations. This hybridization concept was also useful in improving the notch sensitivity, which is another important limiting factor in conventional composite laminates [13].

In order to study the suitability of PDH composites in real-life applications, these composites were investigated at high strain rates and

* Corresponding author.
E-mail address: M.Fotouhi-1@tudelft.nl (M. Fotouhi).

https://doi.org/10.1016/j.compositesa.2022.107206
Received 14 July 2022; Received in revised form 29 August 2022; Accepted 10 September 2022
Available online 16 September 2022

off-axis loadings. QI and UD PDH composites were seen to have excellent pseudo-ductile responses both in quasi-static and high strain rates through fragmentation and stable pull-out of the carbon layers [14]. An increase in the off-axis angle of the QI laminates did cause small changes in the pseudo-ductile strain and maximum stress values, however, the laminates still showed a pseudo-ductile response [15].

As briefly reviewed above, tensile behaviour of the PDH composites has been studied extensively, and a good understanding established; however, in order to apply these composites in real-life applications, their fatigue behaviour should be understood. The complex fatigue failure mechanisms in FRP composites can be attributed to the anisotropic and brittle nature as well as the layered structure of these systems [16,17]. Reviews of fatigue damage assessment in conventional FRP composites can be found in [18,19]. Findings of research on the comparison of tensile fatigue response in basalt/carbon hybrid composites and all basalt fibre composites revealed that the rough surface of the basalt fibre [20] may result in mechanical interlocking between these two fibre types and delayed delamination propagation, thus expanding the fatigue lifetime [21]. The capability of hybridization to cause a beneficial effect on the fatigue resistance of composite laminates was also confirmed by more recent research, where fatigue life of a flax basalt/epoxy hybrid composite was compared to non-hybrid composites [22]. Previously fatigue behaviour of a UD PDH composite was investigated [23], and it was concluded that the UD PDH composite has a good resistance against cyclic loading even after the appearance of damage, and only a gradual increase in damage was observed over thousands of cycles.

However, in practical applications most composite structures require multi-directional pseudo-ductile hybrid laminates. Cutouts and holes are also necessary for the geometry and assembly of these composite sub-components, weakening the laminate [24]. These stress raising geometries have a significant effect on the fatigue life of composites [25–29]. It has been established that the ply and laminate thickness, and hole diameter make a large difference in fatigue loading both in failure stress and damage mechanism [30,31]. Local subcritical damage in PDHs, i.e., dispersed delamination and fragmentation, results in notch insensitivity in quasi-static tensile loading [13]. These subcritical damage mechanisms may act as stress-concentrated areas and weaken the composite's fatigue performance. As a result, there is a need to understand the fatigue behaviour of the multi-directional pseudo-ductile hybrids in both un-notched and notched conditions. Fotouhi et al. [32] briefly presented preliminary results of the fatigue behaviour of one specific QI PDH composite made of carbon/epoxy and glass/epoxy prepregs.

This study provides a comprehensive investigation on the tension–tension fatigue behaviour of two different multi-directional PDHs for both un-notched and open-hole configurations, with varying ply thickness and material properties. HighC was a hybrid of a standard thickness glass fibre prepreg and a thin-ply high strength carbon prepreg, with a carbon to glass thickness ratio of 0.29, whereas LowC was a hybrid of a thin-ply glass fibre prepreg and a high modulus thin carbon fibre prepreg, with a carbon to glass thickness ratio of 0.19. The investigated laminates demonstrated a good fatigue performance with gradual damage growth, showing their applicability for industrial applications. However, the fatigue damage evolution and damage extent, i.e. delamination and fibre fragmentation, were observed to be dependent on the ply thickness, material properties and configurations.

2. Experimental procedures

2.1. Materials and design

Two different types of QI PDHs are investigated using materials from different manufacturers. The first (HighC) is made of thin-ply high modulus M46JB-carbon/epoxy and thin-ply Xstrand-glass/epoxy prepregs, with carbon to glass thickness ratio of 0.29, and the second (LowC) is made of thin-ply high strength T300-carbon/epoxy with a higher failure strain together with a standard-ply S-glass/epoxy prepregs giving a lower ratio of carbon to glass of 0.19. The thin UD Xstrand-glass/513 epoxy and M46JB-carbon/120EP-513 epoxy prepregs were manufactured by North Thin-ply Technology. The UD S-glass/913 epoxy prepreg was supplied by Hexcel. The UD T300/epoxy (SkyFlex USN020A) prepreg was from SK Chemicals (South Korea). Table 1 provides these materials specifications.

A schematic of the investigated lay-up arrangements is illustrated in Fig. 1 and is listed in Table 2, where, in the lay-up column, the first numbers show the orientations of the sub-laminates in degrees.

These lay-up configurations were designed based on damage mode maps (Fig. 2) accounting for the carbon fibre plies' absolute and relative thickness values [6]. Using thin carbon fibre plies, it is possible to achieve pseudo-ductile behaviour in the hybrid composites [36,37], where catastrophic delamination around the first low strain ply failure is avoided and therefore multiple failures in the low strain ply may occur, a damage phenomenon known as fragmentation [38,39]. Damage mode maps are useful and efficient tools showing the effect of different geometric parameters for the given material combinations to find the configuration resulting in optimum pseudo-ductile damage mechanisms, i.e., Fragmentation and Dispersed Delamination (Frag. & Del.).

Table 1
Properties of the prepregs used in this study.

Prepreg type	Xstrand-glass/513 epoxy	M46JB-carbon/513 epoxy [33]	S-glass/913epoxy [6]	T300/120c epoxy[f]
Fibre modulus (GPa)	96[a]	436	88	230 [g]
Prepreg fibre direction Modulus, E11 (GPa)	45.5[b]	233	45.7	101.7
Prepreg transverse direction Modulus, E22 (GPa)	15.4 [31]	7[e]	15.4 [31]	6 [h]
Shear Modulus G_{12} (GPa)	4.34 [31]	4.66[e]	4.34 [31]	2.4 [h]
Poisson's ratio ν_{12}	0.3 [31]	0.3[e]	0.3 [31]	0.3 [h]
Poisson's ratio ν_{21}^{c}	0.102	0.009	0.098	0.021
Fibre failure strain (%)	2.5[b]	0.9	5.5	1.5
Cured nominal thickness (mm)	0.05[b]	0.029	0.155	0.029
Fibre mass per unit area (g/m^2)	75[a]	29	190	22
Fibre volume fraction (%)	42[d]	53	50	43
Supplier	North Thin-ply Technology	North Thin-ply Technology	Hexcel	Sky Flex

Supplier's provided information.
Measured on 16-ply UD laminates, specimens failed explosively at the end tabs.
Poisson's ratio in the 2–1 plane is calculated by using.

$$\vartheta_{21} = \vartheta_{12} \times \frac{E_2}{E_1}$$

Estimated based on UD tensile strength from the experimental data measured on 16 ply UD laminates.
These values are from the datasheet for M40 Carbon/epoxy prepreg with the same resin with relatively similar properties as M46 Carbon/epoxy prepreg.
These values are experimentally measured from a SkyFlex USN020A prepreg with the same matrix and elastic modulus but with a similar type of fibre made by a different manufacturer [1].
This value is based on T300 Data Sheet [34].
The transverse properties were assumed to be equal to the similar USN020A prepreg utilised in Ref. [35], as the data was not available.

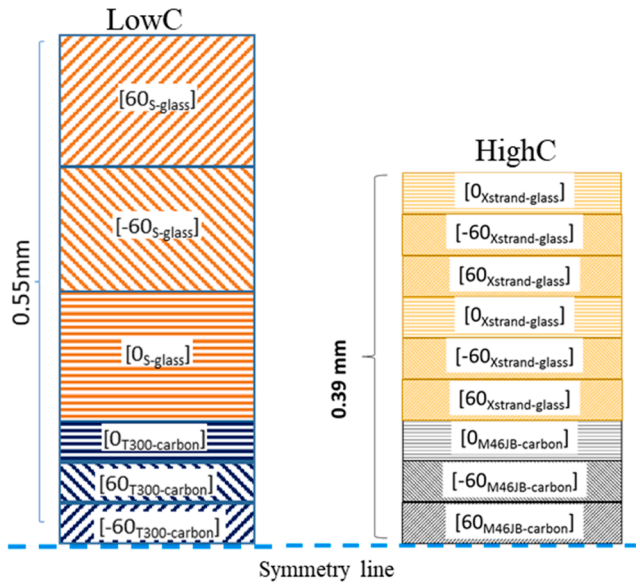

Fig. 1. Schematic of the investigated lay-ups: The yellow, blue, brown, and black colors represent the S-glass, T300-carbon, X-strand-glass, and M46JB-carbon plies, respectively.

Table 2
Thickness and lay-up arrangement of the specimens.

Specimen type	Lay-up arrangement	Laminate thickness [mm]	Carbon to laminate thickness ratio
HighC	$[(0_{Xstrand\text{-}glass}/\text{-}60_{Xstrand\text{-}glass}/60_{Xstrand\text{-}glass})_2/(0_{M46JB\text{-}carbon}/\text{-}60_{M46JB\text{-}carbon}/60_{M46JB\text{-}carbon})]_s$	0.78	0.225
LowC	$[60_{S\text{-}glass}/\text{-}60_{S\text{-}glass}/0_{S\text{-}glass}/0_{T300\text{-}carbon}/60_{T300\text{-}carbon}/\text{-}60_{T300\text{-}carbon}]_s$	1.10	0.157

Herein, the "Relative carbon thickness" and "Carbon thickness" refer to the thickness of all the carbon layers divided by the total thickness of the laminate and the absolute thickness of carbon being sandwiched between the glass layers, respectively. Moreover, different colours demonstrate the expected pseudo-ductile strain amounts. The thickness and proportion of carbon plies in the HighC and LowC configurations are in the Frag. & Del. regions. In this case, the damage mechanisms in the laminates are expected to be fragmentation in the low strain material followed by dispersed delamination and, subsequently, high strain material failure. It is worth mentioning that the represented damage mode maps are related to the un-notched samples, and the damage mechanism in the notched configurations might be different.

2.2. Specimen manufacturing

The resin materials used in the prepregs were 120 EP-513 (North Thin-ply Technology), K50 (SK chemicals) and 913 (Hexcel), with a supplier's recommended curing temperature of 120 °C. End tabs made of 2 mm thick woven glass/epoxy plates supplied by Heathcotes Co. ltd. were bonded to the specimens using a two component Araldite 2000 A/B epoxy adhesive supplied by Huntsman; the components were mixed with the volume fraction ratio of 100: 50 for A: B respectively and cured for 120 min at 80 °C inside a Carbolite oven. A good integrity of the hybrid laminates with no phase separation on cross sectional micrographs was observed, confirming the chemo-mechanical compatibility of the resin systems.

The composite samples were manufactured using a diamond cutting wheel. The open-hole samples were fabricated with a diamond drill on a CNC milling machine (Fig. 3). Visual inspection and repeatable tensile test data of the samples confirmed that no defects or deficiencies were induced by the manufacturing process.

2.3. Test procedure

The un-notched and open-hole specimens were subjected to uniaxial loading with displacement control using a crosshead speed of 1 mm/min for the un-notched laminates and 0.5 mm/min for the open-hole laminates, on a computer controlled Instron 8801 type 100 kN rated universal hydraulic test machine with wedge-type hydraulic grips. It should be noted that different loading rates were used to obtain similar strain rates for the different length specimens, and a shorter length for the notched and open-hole samples, compared with the un-notched samples, was chosen to make more samples from the fabricated plates, optimally using the raw materials and decreasing the manufacturing cost. The length of the specimen away from the notch will not affect the behaviour. To achieve a high resolution in the expected load range, a 25 kN load cell was also utilized.

Tension-tension fatigue tests were performed using the same Instron machine. The pseudo-yield stress (σ_{py}) is defined as the stress level at which the pseudo-ductile damage initiates and the tensile response has a significant deviation from linear elastic behaviour as schematically demonstrated in Fig. 4. Un-notched specimens were fatigued at two different stress levels below σ_{py}, 90 % and 80 %, while open-hole specimens were fatigued at 70 % and 50 % of σ_{py}. Specimens were fatigued until failure or sufficient data acquisition of stiffness reduction was acquired. All fatigue tests were performed under load control by applying a sinusoidal load about the mean load at a frequency of 4 Hz and a stress ratio of 0.1. This is the ratio of the minimum stress (σ_{min}) to

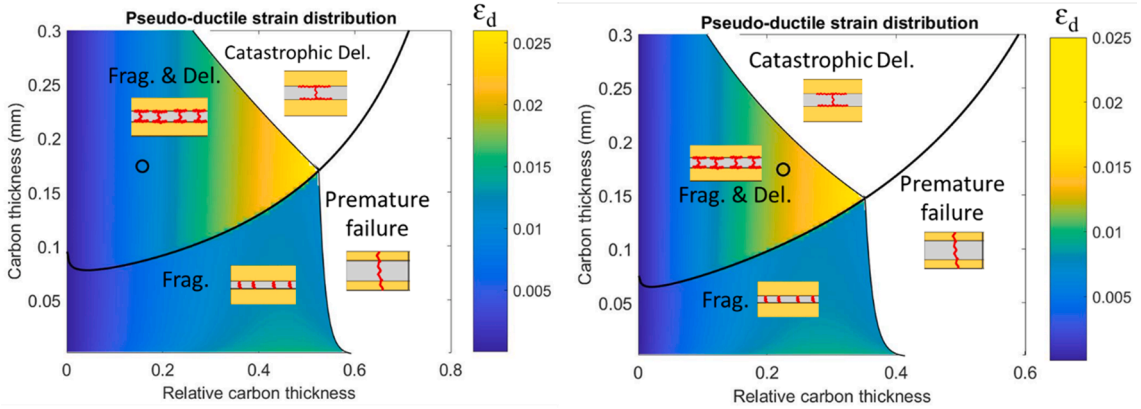

Fig. 2. Distribution of pseudo-ductile strain in the investigated configurations, HighC (right) and LowC (left).

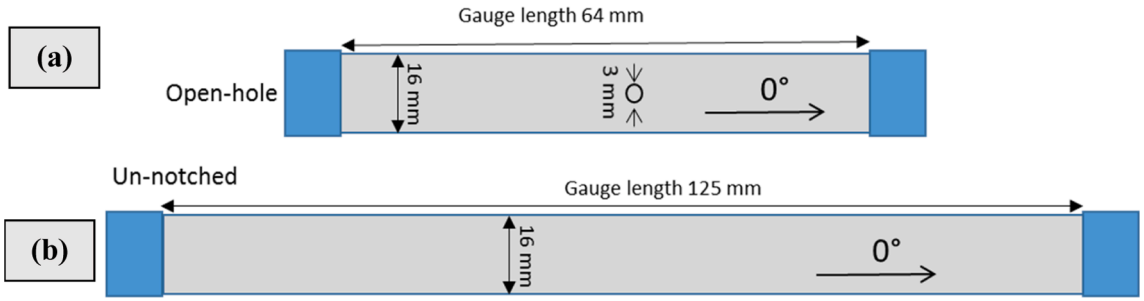

Fig. 3. Schematics of the a) Open-hole, and b) Un-notched specimens.

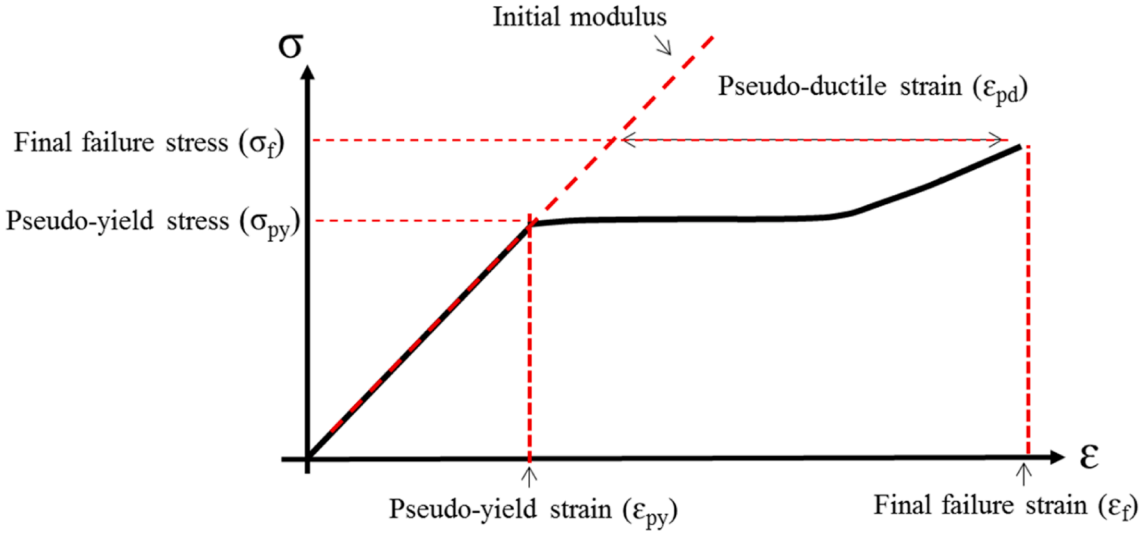

Fig. 4. The stress–strain response of a thin-ply hybrid with Pseudo-ductility.

the maximum stress (σ_{max}) experienced during cyclic loading. Average strains were measured using an Imetrum video gauge system with a 25 mm lens and a nominal gauge length of 125 mm for un-notched samples and 64 mm nominal gauge length for the open-hole samples. Damage growth was monitored using a DSLR vision system with a variable lens and the damage growth area was evaluated with ImageJ software.

2.4. Calculation of the energy release rate

The propensity for delamination growth between the fragmented ply and the intact neighbouring plies is usually characterized by the strain energy release rate. To examine whether catastrophic delamination will occur in the hybrid composite specimens, the strain energy release rate (G_{II}) at the expected failure strain of the low strain material is compared to the mode II fracture toughness of the interface (G_{IIc}). Equation (1) is adopted from the work of Czel et al. [1] to calculate the energy release rate in terms of the carbon stress layer (σ_c):

$$G = \frac{\sigma_c^2 t_c (E_g (t_{total} - t_c) + E_c t_c)}{4 E_g E_c (t_{total} - t_c)} \tag{1}$$

where E is the Young's modulus in the 0°-direction, t is the nominal cured layer thickness for each sublaminate while the subscript g and c refer to the glass and carbon sublaminate plies, respectively. t_{total} is the laminate thickness mentioned in Table 2. The stress in the carbon sublaminate is expressed as σ_c. HighC and LowC comprise glass and carbon plies with a QI sequence with the loading in the 0°-direction, the stiffness in the x-direction (E_x) for the carbon and glass plies is calculated from Classical Laminate Plate Theory shown in Equation (2):

$$E_x = \frac{1}{t}\left(A_{xx} - \frac{A_{xy}^2}{A_{yy}}\right) \tag{2}$$

where t is the thickness of each glass and carbon sublaminate, A_{xx}, A_{xy}, and A_{yy} are the extensional stiffness or in-plane laminate moduli in the xx, xy and yy planes, respectively. The extensional stiffness is calculated from the following Equation (3):

$$A_{ij} = \sum_{k=1}^{n} Q_{ij}^k (t_k - t_{k-1}) \tag{3}$$

where Q_{ij}^k is the stiffness matrix, t_k and t_{k-1} is the thickness of the plies at k and k-1 layers respectively. The second term on the right-hand side in Equation (3) is also known as the nominal cured layer thickness for each sublaminate. The subscript ij refers to the xx, xy, and yy directions. The stiffness matrix is calculated by assuming plane stress conditions. It is possible to expand Equation (3) into Equation (4) as follow:

$$A_{ij=} \sum_{k=1}^{n} \begin{bmatrix} Q_{xx}^k & Q_{xy}^k & 0 \\ Q_{yx}^k & Q_{yy}^k & 0 \\ 0 & 0 & Q_{ss}^k \end{bmatrix} (t_k - t_{k-1}) \tag{4}$$

The stiffness matrix inside the bracket is calculated using Equation (5) to Equation (8), taking into account the properties of the cured ply composite.

$$Q_{xx}^k = \frac{E_1^k}{1 - \vartheta_{12}^k \vartheta_{21}^k} \tag{5}$$

$$Q_{yy}^{k} = \frac{E_2^k}{1 - \vartheta_{12}^k \vartheta_{21}^k} \tag{6}$$

$$Q_{xy}^{k} = Q_{yx}^{k} = \frac{\vartheta_{21}^k E_1^k}{1 - \vartheta_{12}^k \vartheta_{21}^k} = \frac{\vartheta_{12}^k E_2^k}{1 - \vartheta_{12}^k \vartheta_{21}^k} \tag{7}$$

$$Q_{ss}^{k} = G_{12} \tag{8}$$

The properties E_1, E_2, G_{12}, ν_{12}, ν_{21} refer to longitudinal Young's Modulus, transverse Young's Modulus, Major Shear Modulus, Major Poisson's ratios, and Minor Poisson's ratio as listed in Table 1.

The stress in the carbon sublaminate (σ_c) can be expressed in terms of the overall applied stress (σ), with the assumption of equal strain through the thickness of the laminate [1]. Equation (9) is used to calculate the stress in the carbon sublaminate and neglects transverse stresses at the lamina level, since the major Poisson's ratio (ν12) for the glass sublaminate and carbon sublaminate are very similar, as shown in Table 1.

$$\sigma_c = \frac{\sigma t_{total} E_c}{E_g (t_{total} - t_c) + E_c t_c} \tag{9}$$

The notation σ in Equation (9) is defined as the applied fatigue stress level which was 80 % or 90 % of σ_{py} for the un-notched pseudo-ductile hybrid composites and 50 % or 70 % of the notched pseudo-ductile hybrid composites. The growth of delamination under fatigue loading can be described with respect to the cyclic energy release rate (ΔG) [40]:

$$\Delta G = G_{max} - G_{min} \tag{10}$$

where G_{max} and G_{min} refer to the strain energy release rate at the maximum stress (σ_{max}) and minimum stress (σ_{min}) experienced during the cyclic loading. Previous experiments on similar UD hybrid materials comprising the same combinations of epoxy matrix systems as those of this study [1,10,37], indicated that the Hexcel and Sky Flex prepregs have higher mode II toughness (G_{IIc}~1N/mm) than those of the North Thin-ply Technology prepregs (G_{IIc}~0.7 N/mm).

By inserting Equation (3) to Equation (8) into Equation (2), E_{xx} is obtained for each glass and carbon sublaminate plies. Then the stress in the carbon layer for HighC and LowC is calculated using Equation (9). Having fixed the R ratio ($\frac{\sigma_{min}}{\sigma_{max}}$) as 0.1, the maximum stress and minimum stress are calculated by Equation (9). The energy release rate at the maximum (G_{max}) and minimum stress (G_{min}) is then calculated using Equation (1). G_{max} and G_{min} for HighC and LowC are then inserted into Equation (10) to yield the cyclic energy release rate (ΔG) for each hybrid configuration. The cyclic energy release rate for the un-notched HighC loaded at 80 % and 90 % of its respective σ_{py} is 0.4 N/mm and 0.5 N/mm respectively. By comparing the cyclic energy release rate of HighC with the interfacial fracture toughness of around 0.7 N/mm, it is expected that a slow delamination growth would ensue. For the un-notched LowC loaded at 80 % and 90 % of its respective σ_{py}, the cyclic energy release rate is 0.31 N/mm and 0.39 N/mm respectively which is low compared with the interfacial fracture toughness of 1 N/mm. The cyclic energy release rate for the notched HighC loaded at 50 % and 70 % of the un-notched σ_{py} is 0.2 N/mm and 0.37 N/mm, respectively. For the notched LowC loaded at 50 % and 70 % of the un-notched σ_{py}, the cyclic energy release rates are 0.15 N/mm and 0.3 N/mm, respectively. The cyclic energy release rate calculations for the notched samples are done using the net section equivalent stress values of the notched laminates considering the un-notched stress values and the experimentally calculated notch intensity factors reported in Table 3.

3. Results and discussion

3.1. The static tensile behaviour of un-notched and notched specimens

The stress–strain results for the investigated un-notched configurations show an initial linear response followed by deviation from linearity, a plateau, a second linear part and load drop (see Figs. 5-6). The deviation from linearity is marked by a knee-point stress (σ_{py}) as shown in Figs. 5 and 6, where the established fragmentation of the 0° carbon plies is the reason for the appearance of this knee-point [3,8,23]. Dispersed fragmentation and stable pull-out of the fragmented 0° carbon plies from the surrounding plies contribute to the plateau development in both stress–strain curves. When the fragmentation of the carbon plies is saturated and they cannot contribute further to the load-carrying capacity of the hybrid composites, the increase in load is carried by the remaining intact plies causing a rise of stress shown as a second linear part in the stress–strain curves. The final stage is shown as a load drop which indicates the loss of the hybrid composite's structural integrity.

Table 3 summarizes some calculated values of the hybrid configurations. It should be noted that the reported values are averages of six specimen measurements. Due to the higher proportion and stiffness of the carbon layers in the HighC laminate, a higher improvement in the initial modulus is observable compared to the LowC laminate. Higher pseudo-ductile strain and a better load recovery after the plateau were obtained for the LowC laminates compared with HighC. This is due to the lower relative carbon thickness and the better properties of the S-glass layers in the LowC specimens compared with HighC glass layers that had a lower strain to failure.

The stress–strain curves for the open-hole configurations based on the gross-section stress display a linear response followed by a load drop

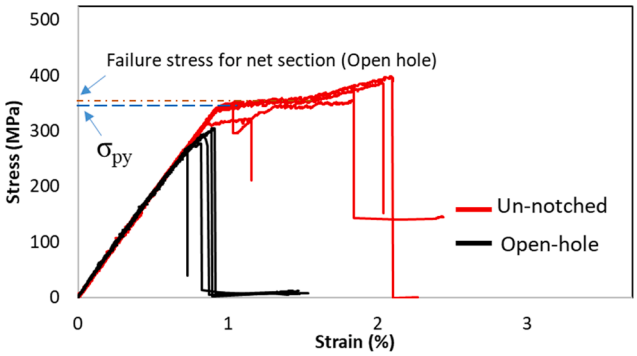

Fig. 5. Results of the tensile tests for HighC samples.

Table 3
Summary of the test results for the un-notched hybrid specimens.

Specimen type	Pseudo-yield strain (%)	Pseudo-yield stress (MPa)	Final failure strain (%)	Pseudo-ductile strain (%)	Final failure stress (MPa)	Initial modulus (GPa)	Improvement in modulus compared to the pure glass (%)	Notch intensity factor (NIF)	Relative carbon to laminate thickness (%)
HighC	0.92 ± 0.05	339 ± 2	1.95 ± 0.14	0.94 ± 0.14	378 ± 18	36.5 ± 0.2	54	0.94	22.5
LowC	1.80 ± 0.02	379 ± 6	3.5 ± 0.10	1.30 ± 0.05	504 ± 18	25.1 ± 0.1	6	0.88	15.7

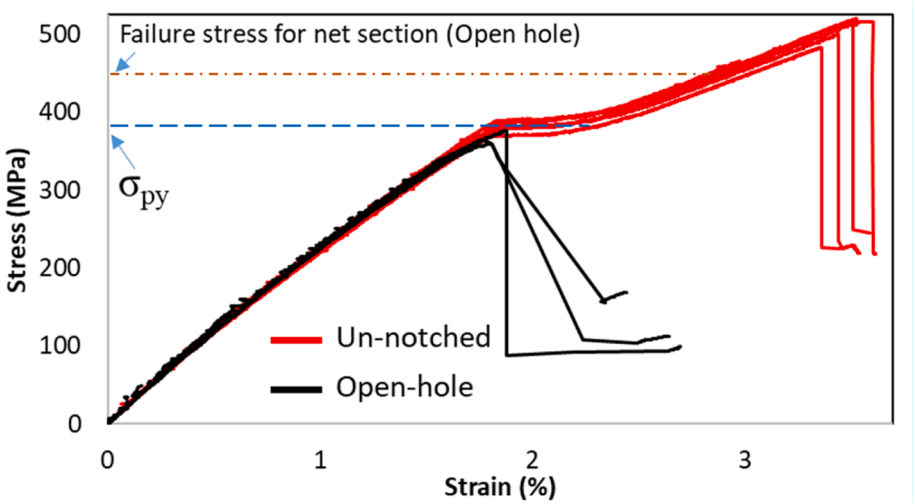

Fig. 6. Results of the tensile tests for LowC samples.

(see Figs. 5 and 6). The Notch Intensity Factor (NIF) value-1 in Table 3, evaluated as the ratio of the net section strength of the open-hole specimen to the un-notched specimen [13], indicates that the net section strength of the laminate does not change significantly due to the existence of the open-hole. The laminates showed reduced notch sensitivity by redistributing stress through subcritical damage mechanisms, i.e. dispersed delamination and fragmentation around the hole tips, as discussed in detail previously [13].

3.2. The fatigue response of un-notched PDH composites

A series of fatigue tests were conducted at two chosen load levels for the un-notched configurations: 80 % and 90 % of the un-notched σ_{py}. The stiffness reductions (E_N/E_o) as a function of number of cycles are shown in Figs. 7 and 8, where E_N is the laminate stiffness at a certain number of cycles and E_o is the initial laminate stiffness at zero cycles. The stiffness without the carbon plies was calculated from the rule of mixtures assuming that the composites lost the whole contribution from the carbon plies. For the HighC fatigued at 80 % of the un-notched σ_{py}, no obvious stiffness reduction was observed up to 100,000 cycles which indicates the absence of damage initiation and development. This is because the applied strain (0.74 %) is well below the static fragmentation strain (0.92 %), and no carbon fibre fragmentation was observed. In addition, both glass and carbon fibre composites in the HighC configuration are thin-plies that can suppress matrix microcracking [1,41,42] thus resulting in negligible stiffness loss. For the LowC, fatigue testing at 80 % of σ_{py} shows a 5 % reduction of the stiffness in the first 10,000 cycles and the laminate lost 9 % of its initial stiffness at 90,000 cycles. When LowC was further fatigued until 100,000 cycles, there was no stiffness reduction and they were still able to sustain the load without failure. LowC was fatigued at 1.44 % strain level that was well below the fragmentation strain (1.80 %), therefore the stiffness reduction of 9 % at 100,000 cycles can be attributed to matrix microcracking, evidenced by visible oblique strips running at an approximate angle of 60° on the laminates surface in Fig. 9, originating from the tensile stress in plies off-axis to the loading direction [43–45].

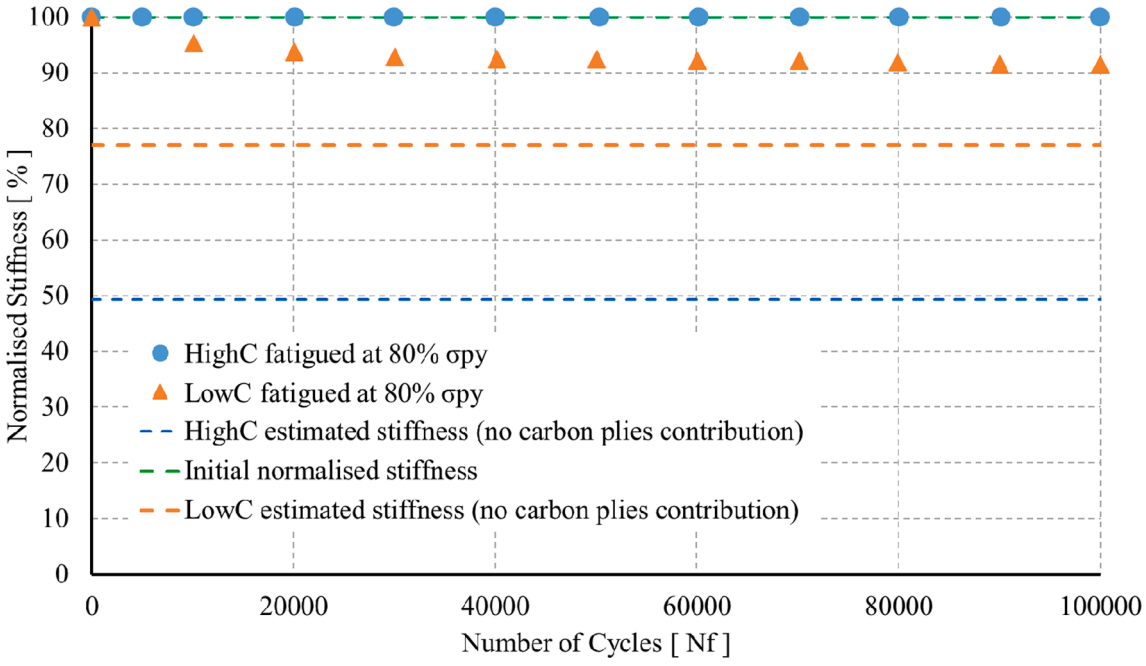

Fig. 7. Normalised stiffness versus number of fatigue cycles for the un-notched laminates fatigued at 80% of the σ_{py}.

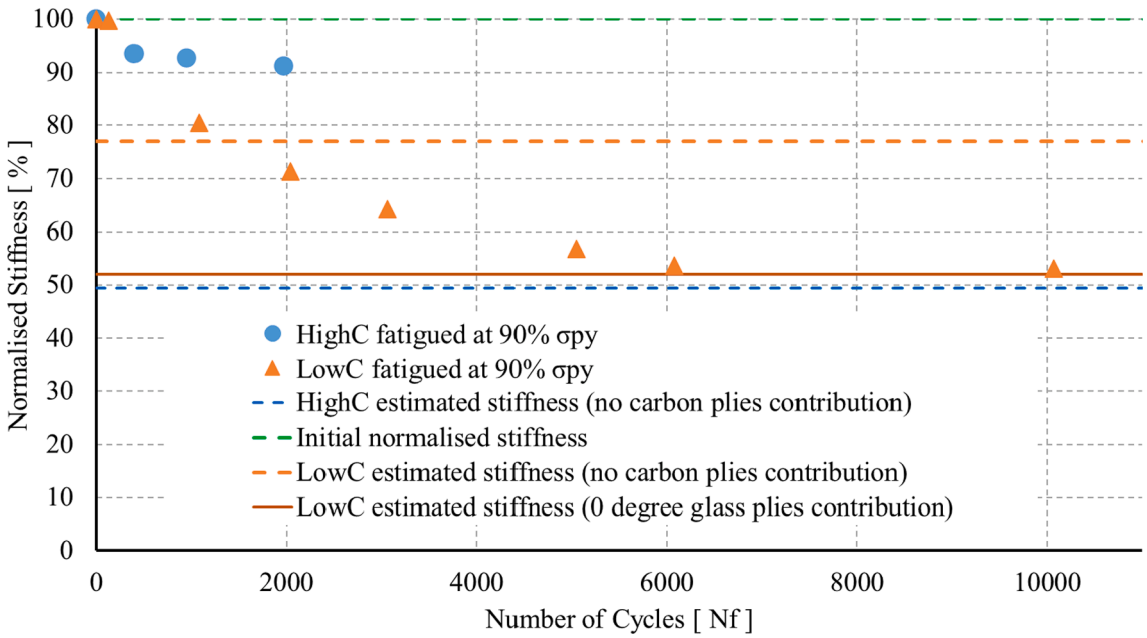

Fig. 8. Normalised stiffness versus number of fatigue cycles for the un-notched laminates fatigued at 90% of the σ_{py}.

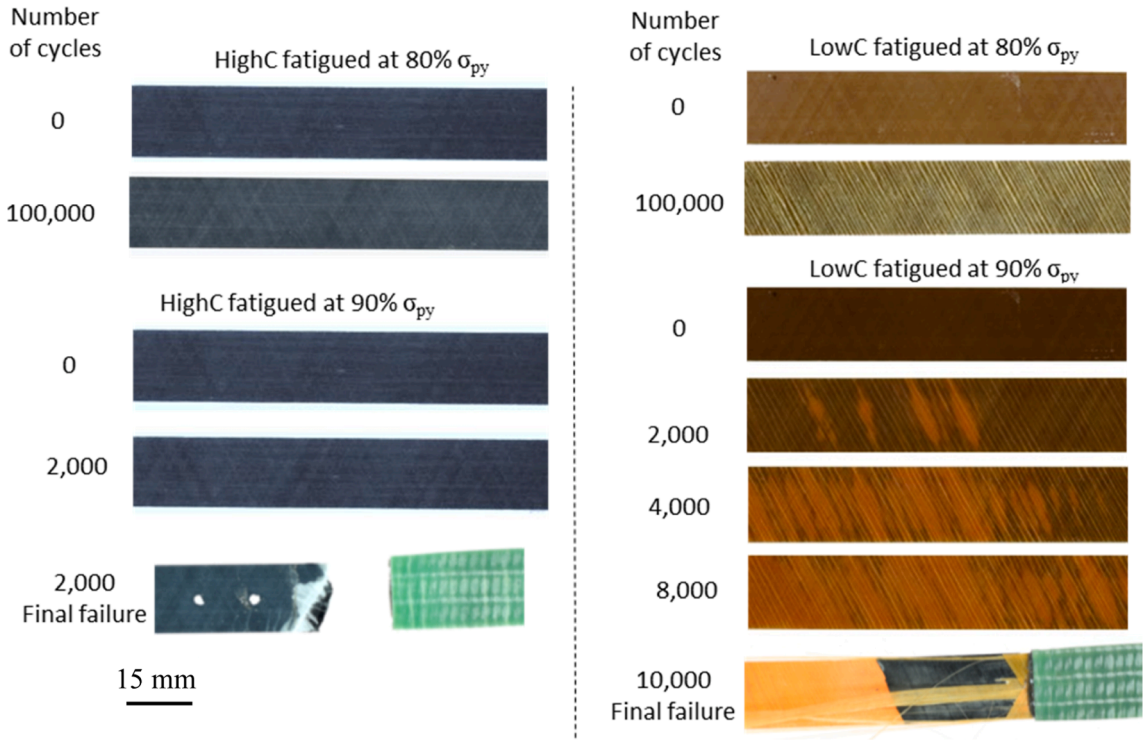

Fig. 9. Typical damage mechanisms for the un-notched HighC and LowC composites.

As seen in Fig. 8., for HighC, when fatigued at 90 % of the σ_{py}, the strain level is at 0.83 %, a stiffness reduction of 9 % was recorded at around 2000 cycles and a sudden failure occurred after that number of cycles. Although no visible damage was observed on the specimen before the failure, it is expected that the stiffness reduction can be attributed to the carbon fibre fragmentation. This is because the strain level of 0.83 % is apparently within the statistical range for carbon fracture to take place, so most likely HighC had some limited fragmented 0° carbon plies that did not result in delamination. The final stiffness for HighC without the carbon contribution is 48 % and the final stiffness without the carbon and 60-degree Xstrand-glass plies is 33 %. As shown in Fig. 8, the final stiffness of the HighC never reached the reduced stiffness without the carbon plies' contribution. This reflects that the carbon plies did not reach fully saturated fragmentation or delamination and the fragmented carbon plies could still contribute to the stiffness. HighC has a cyclic energy release rate of 0.5 N/mm, compared with the interfacial fracture toughness (0.7 N/mm), and no delamination was observed during fatigue loading. The thin carbon and thin glass plies can suppress matrix microcracking [41,42,46] and keep the stresses concentrated around the fractured carbon plies until a catastrophic

failure occurs after about 2000 cycles.

When LowC was fatigued at 90 % of the un-notched σ_{py}, a significant stiffness reduction of 47 % was recorded at 10,000 cycles just before the final failure. The stiffness without the carbon contribution is 77 % and the final stiffness without the carbon and 60-degree S-glass plies contribution is 52 %. The final stiffness of LowC went below the stiffness without the carbon plies contribution which means that the laminates have lost the stiffness contribution from the carbon plies and the glass plies off-axis to the loading direction due to matrix microcracking. This is in agreement with the literature review [43–45], where transverse matrix cracking was attributed to the stiffness loss in conventional QI laminates. It is evident that at 90 % of the un-notched σ_{py}, the applied strain level of 1.63 % is within the statistical range for carbon fracture to take place, resulting in fragmentation of the 0° carbon plies during fatigue loading, followed by delamination between the 0° carbon plies and the remaining intact plies. A similar behavior was observed by Suwarta, et. al. [23] for the stiffness loss of UD thin-ply hybrid composites made of thin-ply TC35 carbon/epoxy composites sandwiched between standard thickness S-Glass/913 epoxy composite. Based on their experimental work, it was observed that when UD hybrid specimens are fatigued at 90 % of σ_{py}, TC35 fragmentations and growth of delamination from the fragmentations caused stiffness reduction as the number of cycles increases. As shown in Fig. 9, the delaminated areas observed during fatigue loading grew gradually with an increasing number of fatigue cycles and eventually joined the neighbouring delaminated areas. Delamination is visible as the lighter areas due to the translucent nature of the glass/epoxy outer layers of the hybrid composites and the well bonded areas appear black. Due to a large difference between the cyclic energy release rate (0.39 N/mm) compared with the interfacial fracture toughness (1 N/mm) in the LowC, the delamination grew very slowly with advancing number of cycles. This growing delaminated area shown as the lighter areas is also running at an approximate angle of 60° which correlates with the angle of the S-Glass outer layer. The probable explanation for the angle of the delaminated area is delamination originating from the off-axis glass plies, beside the delamination between the 0° T300 carbon layer and 0° S-Glass/913 layer originating

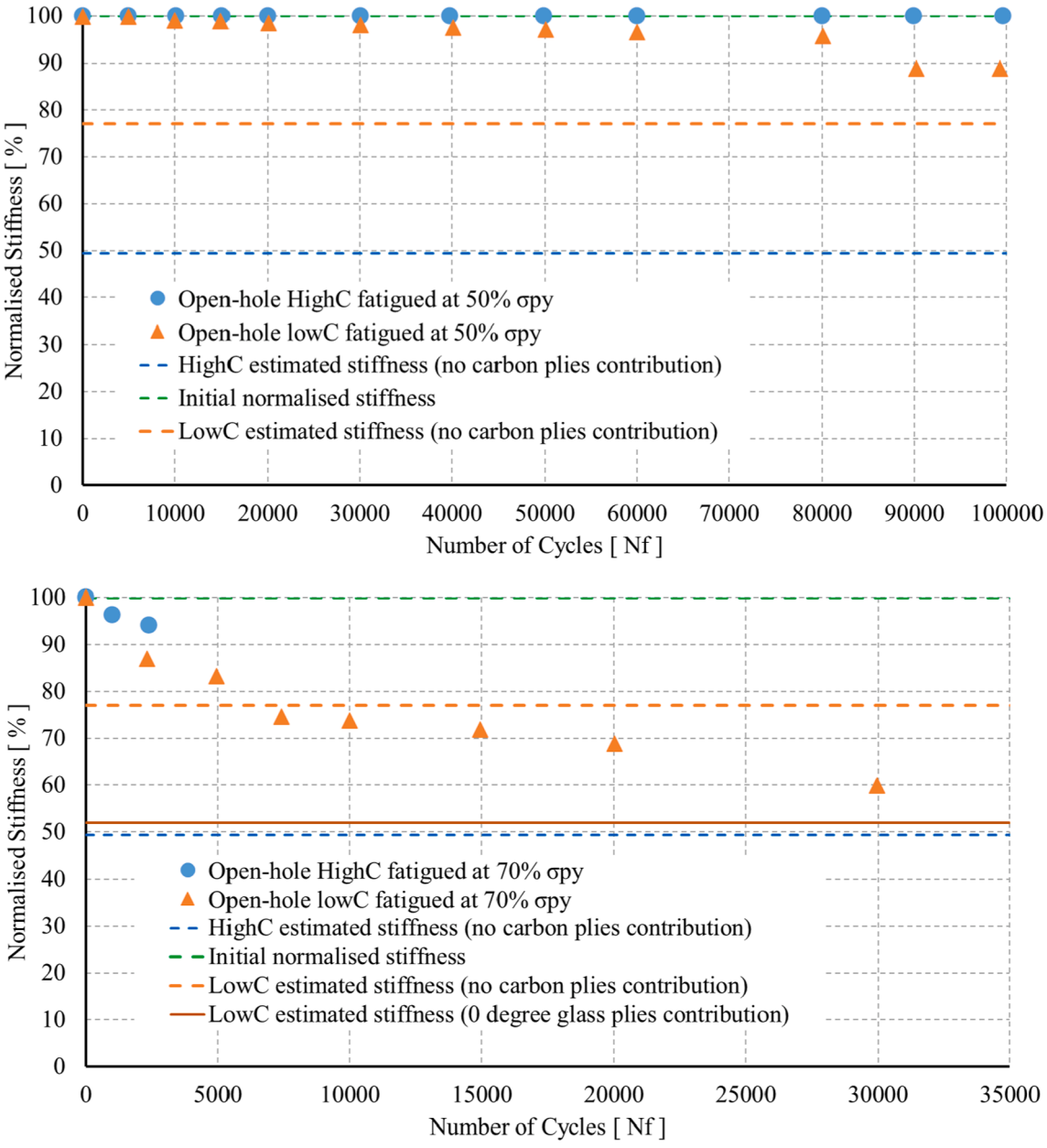

Fig. 10. Relation between stiffness loss and increasing number of fatigue cycles for open-hole LowC and HighC fatigued at 50% and 70% of the un-notched σ_{py}.

from the fragmented 0° carbon plies. The matrix microcracking occurs because of the high tensile stresses in plies off-axis to the loading direction [47–49]. LowC specimens experience higher strain levels compared with HighC samples at the given stress levels, almost 80 % and 90 % of the respective Pseudo-yield strains (%) listed in Table 3. As a result, for a given stress level, the matrix cracking and delamination damage initiation and propagation in HighC is restricted, whereas LowC samples experience earlier matrix cracking and delamination. Please note that there are two white dots on the bottom left of Fig. 9 which are created by a white marker for strain measurements.

3.3. The fatigue response of the open-hole PDH composites

Fig. 10 shows the results for the open-hole laminates that were fatigued at 50 % and 70 % of the un-notched σ_{py}. The damage mechanisms observed at different numbers of cycles for the open-hole laminates fatigued at 50 % and 70 % of the un-notched σ_{py} are illustrated in Fig. 11.

For the open-hole HighC at 50 % σ_{py} of the un-notched σ_{py}, there was negligible stiffness reduction up until 100,000 cycles. From Fig. 11, there is no obvious damage or delamination seen on the surface of this hybrid specimen which is consistent with the negligible stiffness reduction up until 100,000 cycles. Previous work [13]on the tensile tests of the open-hole samples showed that the stress concentration around the hole, $\sigma_{nom}/\sigma_{max} = 3.13$ calculated from the theoretical stress concentration factor, results in some invisible damage around the hole of the HighC and LowC samples at a strain level of around 70 %. However, the damage events occur only locally at the hole vicinity and do not change the overall stiffness. For the HighC open-hole laminates fatigued at 70 % of the un-notched σ_{py}, a 5 % reduction of normalised stiffness was recorded at 3000 cycles after which sudden failure occurred as shown in Fig. 10. For this hybrid configuration, the stiffness before the final failure never reached the estimated stiffness with no carbon ply contribution. Although the strain level at 70 % of σ_{py} is below the statistical range for carbon fracture to take place without a notch, the 3.13 stress concentration around the hole would facilitate damage initiation and growth [47]. In HighC delamination damage propagates from the fractured carbon plies due to the difference between the cyclic energy release rate at 70 % of the un-notched σ_{py} (0.31 N/mm) compared with the interfacial fracture toughness (0.7 N/mm). The delamination propagates across the width, reducing the effective cross section, and the laminate can no longer tolerate the damage resulting in a sudden brittle fibre failure. The final failure of the open-hole HighC fatigued at 70 % σ_{py} is a typical brittle failure. This brittle failure type for the thin-ply composites was also reported by other researchers [41,42,46]. The delamination size can be seen as the lighter area, this small delamination size is attributed to the ability of both Xstrand-glass and M46JB thin-plies to suppress matrix microcracking and delamination initiated by the local fibre failure near the hole [1,41,42]. The open-hole HighC fatigued at 50 % σ_{py} did not fail after 100,000 cycles.

When the open-hole LowC was fatigued at 50 % of the un-notched σ_{py}, it was observed that the stiffness of this laminate gradually decreases up to around 10 % of the initial stiffness at 90,000 cycles. From Fig. 11, there are some visible oblique stripes that are associated with matrix microcracking originating from the tensile stress in plies off-axis to the loading direction [44–46], causing the stiffness reduction for the open-hole LowC. For the un-notched LowC, the laminate lost 9 % from its initial stiffness at 90,000 cycles which is similar to the stiffness reduction of the notched LowC fatigued at 50 % of the un-notched σ_{py}. Whereas for LowC fatigued at 70 %, a gradual stiffness reduction was observed up until 30,000 cycles when a reduction of 41 % was recorded, as shown in Fig. 10. Similar to the un-notched sample, the normalised stiffness of the open-hole LowC went below the estimated stiffness with no carbon plies contribution. This is because as well as the damage mechanisms of fragmentation of the T300 carbon layer, and delamination between the 0° T300 carbon layer and 0° S-Glass/913 layer, there was matrix microcracking and associated delamination in the glass plies off-axis to the loading direction. The open-hole LowC did experience final fibre failure as well, however, there is a significant area of delamination and matrix cracking before the final fibre failure as shown in Fig. 11. There is a large difference between the cyclic energy release rate (0.3 N/mm) compared with the interfacial fracture toughness (1 N/mm), in the LowC fatigued at 70 %, helping to avoid sudden failure and to release the high stress concentration around the hole by fragmentation and dispersed delamination of the carbon plies, which prolongs the fatigue life of the open-hole LowC.

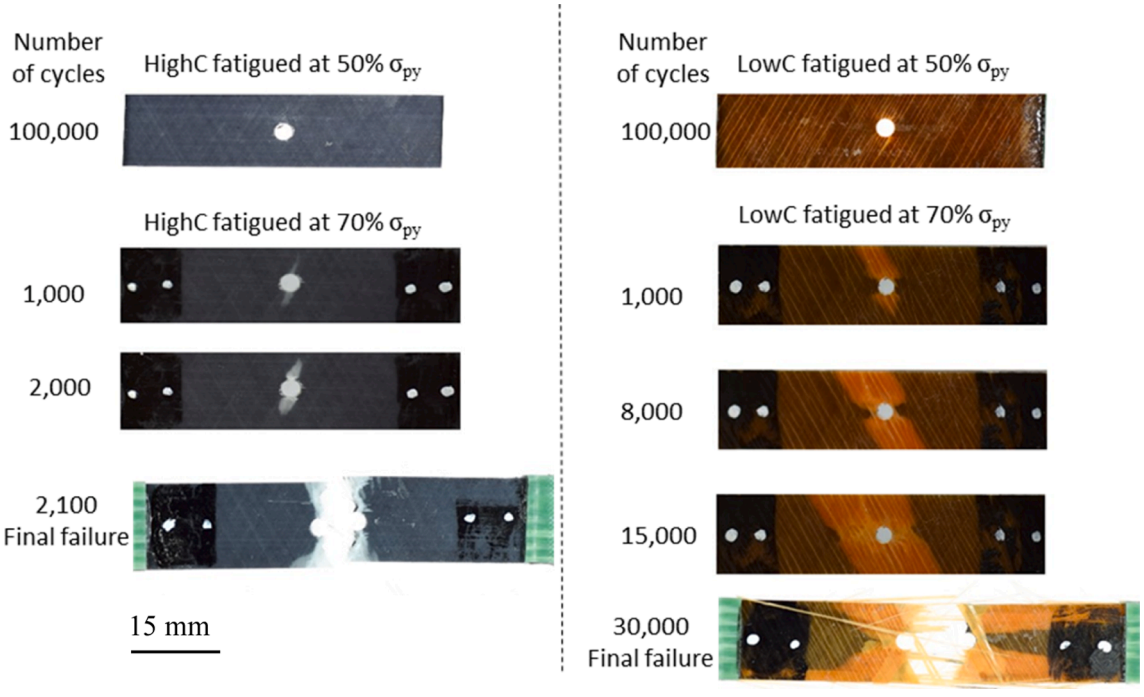

Fig. 11. (a) Typical damage mechanisms for the open-hole laminates fatigued at 50% of σ_{py} and 70% of σ_{py}.

4. Conclusions

This paper provides a comprehensive investigation of the static tension and tension–tension fatigue behaviour of two different quasi-isotropic pseudo-ductile thin-ply carbon/glass epoxy hybrid composites. An understanding of the fatigue performance is accomplished, highlighting the key parameters affecting the fatigue behaviour. The important key parameters are the ply thickness, the cyclic energy release rate and the interfacial fracture toughness. Un-notched and open-hole configurations with different ply thicknesses and material properties are examined and the following is concluded:

- A successful pseudo-ductile un-notched behaviour which also showed notch-insensitivity was achieved through subcritical pseudo-ductile damage mechanisms, i.e. fragmentation and dispersed delamination.
- The investigated laminates demonstrated a good fatigue performance with no sudden failure up to 100,000 cycles when fatigued well below the carbon layer fracture strain, i.e. at 80 % of σ_{py} for the un-notched configuration and 50 % of σ_{py} for the open-hole configuration.
- The un-notched LowC fatigued at 80 % of the σ_{py} experienced some matrix cracking and stiffness reduction, whereas the HighC did not experience any visible damage and stiffness reduction.
- By increasing the stress level to 90 % of the σ_{py}, there is a gradual stiffness reduction due to the appearance of matrix cracking, fragmentation and dispersed delamination in the un-notched LowC. Whereas there is no visible damage such as matrix cracking for HighC, however, there is some stiffness reduction due to fragmentation of the carbon fibre, and the final failure is more brittle and happens at a lower number of cycles compared with LowC.
- For the open-hole laminates (fatigued at 70 % of the σ_{py}), fragmentation and delamination release the stress concentration and the delamination then spreads gradually across the width of the specimen. A larger number of cycles and a higher damage area were observed before the final failure for LowC in comparison with HighC.
- Different fatigue behaviours in HighC and LowC are attributed to the lower amount of carbon and a larger difference between the G_{IIc} value and the cyclic energy release rate in LowC, making the laminate more damage tolerant and redistributing the stress/damage over a larger area resulting in a gradual failure.
- Due to the translucent nature of the glass layers, the damage evolution during the fatigue test of the investigated hybrids was observable with a naked eye, allowing in-situ inspection of the damage and correlating it with the stiffness reduction of the laminates.

CRediT authorship contribution statement

Mohamad Fotouhi: Conceptualization, Supervision, Methodology, Investigation, Data curation, Writing – original draft, Funding acquisition. **Putu Suwarta:** Data curation, Writing – original draft. **Ali Tabatabaeian:** Writing – original draft, Writing – review & editing. **Sakineh Fotouhi:** Writing – original draft, Writing – review & editing. **Ross Jenkin:** Data curation. **Meisam Jalalvand:** Conceptualization, Writing – review & editing. **Michael R. Wisnom:** Conceptualization, Supervision, Funding acquisition.

Declaration of Competing Interest

The authors declare that they have no known competing financial interests or personal relationships that could have appeared to influence the work reported in this paper.

Data availability

Data will be made available on request.

Acknowledgements

This work was funded under the UK Engineering and Physical Sciences Research Council (EPSRC) Grants; EP/V009451/1 on Next generation of high-performance impact resistant composites with visibility of damage, and the Programme Grant EP/I02946X/1 on High Performance Ductile Composite Technology in collaboration with Imperial College. The data necessary to support the conclusions are included in the paper.

References

[1] Czél G, Wisnom MR. Demonstration of pseudo-ductility in high performance glass/epoxy composites by hybridisation with thin-ply carbon prepreg. Compos A Appl Sci Manuf 2013;52:23–30. https://doi.org/10.1016/j.compositesa.2013.04.006.
[2] Swolfs Y, Meerten Y, Hine P, Ward I, Verpoest I, Gorbatikh L. Introducing ductility in hybrid carbon fibre/self-reinforced composites through control of the damage mechanisms. Compos Struct 2015;131:259–65. https://doi.org/10.1016/j.compstruct.2015.04.069.
[3] Czél G, Jalalvand M, Wisnom MR. Design and characterisation of advanced pseudo-ductile unidirectional thin-ply carbon/epoxy-glass/epoxy hybrid composites. Compos Struct 2016;143:362–70. https://doi.org/10.1016/j.compstruct.2016.02.010.
[4] Yuan F, Chen M, Pan J. Experimental study on seismic behaviours of hybrid FRP–steel-reinforced ECC–concrete composite columns. Compos B Eng 2019;176:107272.
[5] Dlugosch M, Fritsch J, Lukaszewicz D, Hiermaier S. Experimental investigation and evaluation of numerical modeling approaches for hybrid-FRP-steel sections under impact loading for the application in automotive crash-structures. Compos Struct 2017;174:338–47. https://doi.org/10.1016/j.compstruct.2017.04.077.
[6] Jalalvand M, Czél G, Wisnom MR. Damage analysis of pseudo-ductile thin-ply UD hybrid composites - A new analytical method. Compos A Appl Sci Manuf 2015;69:83–93. https://doi.org/10.1016/j.compositesa.2014.11.006.
[7] Callens MG, Gorbatikh L, Verpoest I. Ductile steel fibre composites with brittle and ductile matrices. Compos A Appl Sci Manuf 2014;61:235–44. https://doi.org/10.1016/j.compositesa.2014.02.006.
[8] Fotouhi M, Suwarta P, Jalalvand M, Czel G, Wisnom MR. Detection of fibre fracture and ply fragmentation in thin-ply UD carbon/glass hybrid laminates using acoustic emission. Compos A Appl Sci Manuf 2016;86:66–76.
[9] Callens MG, De Cuyper P, Gorbatikh L, Verpoest I. Effect of fibre architecture on the tensile and impact behaviour of ductile stainless steel fibre polypropylene composites. Compos Struct 2015;119:528–33. https://doi.org/10.1016/j.compstruct.2014.09.028.
[10] Czél G, Rev T, Jalalvand M, Fotouhi M, Longana ML, Nixon-Pearson OJ, et al. Pseudo-ductility and reduced notch sensitivity in multi-directional all-carbon/epoxy thin-ply hybrid composites. Compos A Appl Sci Manuf 2018;104:151–64.
[11] Jalalvand M, Fotouhi M, Wisnom MR. Orientation-dispersed pseudo-ductile hybrid composite laminates – A new lay-up concept to avoid free-edge delamination. Compos Sci Technol 2017;153:232–40. https://doi.org/10.1016/j.compscitech.2017.10.011.
[12] Fotouhi M, Jalalvand M, Wisnom MR. High performance quasi-isotropic thin-ply carbon/glass hybrid composites with pseudo-ductile behaviour in all fibre orientations. Compos Sci Technol 2017;152:101–10. https://doi.org/10.1016/j.compscitech.2017.08.024.
[13] Fotouhi M, Jalalvand M, Wisnom MR. Notch insensitive orientation-dispersed pseudo-ductile thin-ply carbon/glass hybrid laminates. Compos A Appl Sci Manuf 2018;110:29–44. https://doi.org/10.1016/j.compositesa.2018.04.012.
[14] Fotouhi M, Fuller J, Longana M, Jalalvand M, Wisnom MR. The high strain rate tension behaviour of pseudo-ductile high performance thin ply composites. Compos Struct 2019;215:365–76.
[15] Fotouhi M, Jalalvand M, Saeedifar M, Xiao B, Wisnom MR. High performance quasi-isotropic thin-ply carbon/glass hybrid composites with pseudo-ductile behaviour loaded off-axis. Compos Struct 2020;247:112444. https://doi.org/10.1016/j.compstruct.2020.112444.
[16] Tsai SN, Carolan D, Sprenger S, Taylor AC. Fracture and fatigue behaviour of carbon fibre composites with nanoparticle-sized fibres. Compos Struct 2019;217:143–9. https://doi.org/10.1016/j.compstruct.2019.03.015.
[17] Capela C, Oliveira SE, Ferreira JAM. Fatigue behavior of short carbon fiber reinforced epoxy composites. Compos B Eng 2019;164:191–7. https://doi.org/10.1016/j.compositesb.2018.11.035.
[18] Shabani P, Taheri-Behrooz F, Samareh-Mousavi SS, Shokrieh MM. Very high cycle and gigacycle fatigue of fiber-reinforced composites: A review on experimental approaches and fatigue damage mechanisms. Prog Mater Sci 2021;118:100762. https://doi.org/10.1016/j.pmatsci.2020.100762.
[19] Gaurav A, Singh KK. Fatigue behavior of FRP composites and CNT-Embedded FRP composites: A review. Polym Compos 2018;39:1785–808. https://doi.org/10.1002/pc.24177.

[20] Militký J, Kovačič V, Rubnerová J. Influence of thermal treatment on tensile failure of basalt fibers. Eng Fract Mech 2002;69:1025–33. https://doi.org/10.1016/S0013-7944(01)00119-9.
[21] Wu Z, Wang X, Iwashita K, Sasaki T, Hamaguchi Y. Tensile fatigue behaviour of FRP and hybrid FRP sheets. Compos B Eng 2010;41:396–402. https://doi.org/10.1016/j.compositesb.2010.02.001.
[22] Seghini MC, Touchard F, Sarasini F, Chocinski–Arnault L, Ricciardi MR, Antonucci V, et al. Fatigue behaviour of flax-basalt/epoxy hybrid composites in comparison with non-hybrid composites. Int J Fatigue 2020;139:105800.
[23] Suwarta P, Fotouhi M, Czél G, Longana M, Wisnom MR. Fatigue behaviour of pseudo-ductile unidirectional thin-ply carbon/epoxy-glass/epoxy hybrid composites. Compos Struct 2019;224:110996.
[24] Van Der Sypt P, Chérif M, Bois C. Analysis of the fatigue behaviour of laminated composite holes subjected to pin-bearing loads. Int J Fatigue 2017;103:86–98. https://doi.org/10.1016/j.ijfatigue.2017.05.025.
[25] Aidi B, Philen MK, Case SW. Progressive damage assessment of centrally notched composite specimens in fatigue. Compos A Appl Sci Manuf 2015;74:47–59. https://doi.org/10.1016/j.compositesa.2015.03.022.
[26] Shabani P, Taheri-Behrooz F, Maleki S, Hasheminasab M. Life prediction of a notched composite ring using progressive fatigue damage models. Compos B Eng 2019;165:754–63. https://doi.org/10.1016/j.compositesb.2019.02.031.
[27] Qiao Y, Deleo AA, Salviato M. A study on the multi-axial fatigue failure behavior of notched composite laminates. Compos A Appl Sci Manuf 2019;127:105640. https://doi.org/10.1016/j.compositesa.2019.105640.
[28] Qiao Y, Salviato M. Micro-computed tomography analysis of damage in notched composite laminates under multi-axial fatigue. Compos B Eng 2020;187:107789. https://doi.org/10.1016/j.compositesb.2020.107789.
[29] Ghasemi AR, Tabatabaeian A, Moradi M. A new insight into impact of thermal cycling on the un-notched and circular hole polymeric composite rings via naval ordnance laboratory-ring test. J Compos Mater 2020;54(23):3287–95.
[30] Muc A, Romanowicz P. Effect of notch on static and fatigue performance of multilayered composite structures under tensile loads. Compos Struct 2017;178:27–36. https://doi.org/10.1016/j.compstruct.2017.07.004.
[31] Hallett SR, Green BG, Jiang WG, Wisnom MR. An experimental and numerical investigation into the damage mechanisms in notched composites. Compos A Appl Sci Manuf 2009;40:613–24. https://doi.org/10.1016/j.compositesa.2009.02.021.
[32] Fotouhi M, Suwarta P, Jenkin R, Jalalvand M, Wisnom M. Fatigue behavior of un-notched and open-hole quasi-isotropic pseudo-ductile thin-ply carbon/glass hybrid laminates. ICCM International Conferences on Composite Materials 2019;2019-Augus.
[33] Czél G, Jalalvand M, Wisnom M. Pseudo-ductile carbon/epoxy hybrid composites. ICCM International Conferences on Composite Materials, vol. 2015- July, 2015.
[34] Toray carbon fibers America INC. T300 data sheet No. CFA-001 n.d. www.toray.com.
[35] Fuller J, Wisnom M. Damage suppression in thin ply angle-ply carbon/epoxy laminates. 19th Int. Conf. Compos. Mater., Montreal , 2013.
[36] Czél G, Jalalvand M, Wisnom MR. Demonstration of pseudo-ductility in unidirectional hybrid composites made of discontinuous carbon/epoxy and continuous glass/epoxy plies. Compos A Appl Sci Manuf 2015;72:75–84. https://doi.org/10.1016/j.compositesa.2015.01.019.
[37] Czél G, Jalalvand M, Wisnom MR, Czigány T. Design and characterisation of high performance, pseudo-ductile all-carbon/epoxy unidirectional hybrid composites. Compos B Eng 2017;111:348–56. https://doi.org/10.1016/j.compositesb.2016.11.049.
[38] Wisnom MR, Czél G, Swolfs Y, Jalalvand M, Gorbatikh L, Verpoest I. Hybrid effects in thin ply carbon/glass unidirectional laminates: Accurate experimental determination and prediction. Compos A Appl Sci Manuf 2016;88:131–9.
[39] Mesquita F, Swolfs Y, Lomov SV, Gorbatikh L. Ply fragmentation in unidirectional hybrid composites linked to stochastic fibre behaviour: A dual-scale model. Compos Sci Technol 2019;181:107702. https://doi.org/10.1016/j.compscitech.2019.107702.
[40] Wisnom MR, Jones M. Delamination of unidirectional glass fibre-epoxy with cut plies loaded in four point bending. J Reinf Plast Compos 1995;14:45–59. https://doi.org/10.1177/073168449501400103.
[41] Amacher R, Cugnoni J, Botsis J, Sorensen L, Smith W, Dransfeld C. Thin ply composites: Experimental characterization and modeling of size-effects. Compos Sci Technol 2014;101:121–32. https://doi.org/10.1016/j.compscitech.2014.06.027.
[42] Sihn S, Kim RY, Kawabe K, Tsai SW. Experimental studies of thin-ply laminated composites. Compos Sci Technol 2007;67:996–1008. https://doi.org/10.1016/j.compscitech.2006.06.008.
[43] Tong J, Guild FJ, Ogin SL, Smith PA. On matrix crack growth in quasi-isotropic laminates – I. Experimental investigation. Compos Sci Technol 1997;57:1527–35. https://doi.org/10.1016/S0266-3538(97)00080-8.
[44] Behera A, Thawre MM, Ballal A. Effect of matrix crack generation on Fatigue life of CFRP multidirectional laminates. Mater Today: Proc 2018;5:20078–84. https://doi.org/10.1016/j.matpr.2018.06.374.
[45] Nairn JA. Matrix Microcracking in Composites. Comprehensive Composite Materials 2000;2:403–32. https://doi.org/10.1016/b0-08-042993-9/00069-3.
[46] Saito H, Takeuchi H, Kimpara I. A study of crack suppression mechanism of thin-ply carbon-fiber-reinforced polymer laminate with mesoscopic numerical simulation. J Compos Mater 2014;48(17):2085–96.
[47] Nixon-pearson OJ, Hallett SR, Withers PJ, Rouse J. Damage development in open-hole composite specimens in fatigue. Part 1: Experimental investigation. Compos Struct 2013;106:882–9. https://doi.org/10.1016/j.compstruct.2013.05.033.
[48] Nixon-Pearson OJ, Hallett SR. An experimental investigation into quasi-static and fatigue damage development in bolted-hole specimens. Compos B 2015;77:462–73. https://doi.org/10.1016/j.compositesb.2015.03.051.
[49] Nixon-Pearson OJ, Hallett SR. Composites : Part A An investigation into the damage development and residual strengths of open-hole specimens in fatigue. Compos A 2015;69:266–78. https://doi.org/10.1016/j.compositesa.2014.11.013.